Phase Transitions and Criticality in Small Systems: Vapor−Liquid Transition in Nanoscale Spherical Cavities

Alexander V. Neimark* and Aleksey Vishnyakov

Center for Modeling and Characterization of Nanoporous Materials, TRI/Princeton, 601 Prospect Avenue, Princeton, New Jersy 08542

Received: November 6, 2005; In Final Form: February 6, 2006

Phase transformations in fluids confined to nanoscale pores, which demonstrate characteristic signatures of first-order phase transitions, have been extensively documented in experiments and molecular simulations. They are characterized by a pronounced hysteresis, which disappears above a certain temperature. A rigorous interpretation of these observations represents a fundamental problem from the point of view of statistical mechanics. Nanoscale systems are essentially small, finite volume systems, in which the concept of the thermodynamic limit is no longer valid, and the statistical ensembles are not equivalent. Here, we present a rigorous approach to the description and molecular simulations of phase transitions and criticality in small confined systems, as illustrated by the example of vapor−liquid transition (capillary condensation) in spherical cavities. The method is based on the analysis of the canonical ensemble isotherms, which can be generated by the gauge cell Monte Carlo simulation method. The method allows one to define the critical temperature of phase transition, conditions of phase equilibrium, limits of stability of metastable states, and nucleation barriers, which determine hysteretic phase transformations.

1. Introduction

Starting in the 1960s, thermodynamics of equilibrium and phase behavior in small systems has been at the center of scientific controversy.[1−11] Phase transformations in small systems, which demonstrate characteristic signatures of first-order phase transitions, have been extensively analyzed in experiments and molecular simulations of various systems ranging from nuclei to molecular clusters to nanoconfined fluids.[12−17] Recently, the processes of capillary condensation/evaporation and freezing/melting of fluids in nanoscale pores and nanoporous materials have come into focus. As shown in numerous experiments,[18−28] Monte Carlo (MC) and Molecular Dynamics (MD) simulations,[29−33] and density functional theory calculations,[34−36] these processes are characterized by a pronounced hysteresis, which disappears above a certain temperature. However, a rigorous statisticomechanical interpretation of these observations poses a fundamental problem. Nanoscale systems are essentially small, finite volume systems, in which the thermodynamic functions are analytical so that the very definition of phase transitions, which in macroscopic systems are associated with nonanalyticities of the respective thermodynamic potentials, has to be revisited.[7,14,37−40] The concept of the thermodynamic limit is no longer valid, and the statistical mechanical ensembles (microcanonical, canonical, and grand canonical) are not equivalent.[2,3,9,10,41,42]

In this work, we present a rigorous approach to the description and molecular simulations of phase transitions and criticality in small confined systems, which is illustrated by the example of vapor−liquid transition (capillary condensation) in nanoscale pores. Our approach is based on the analysis of the canonical ensemble isotherms, which can be generated by the gauge cell MC simulation method.[43,44] In the application of this method, the critical temperature of the phase transition, the conditions of phase equilibrium, the limits of stability of metastable states, and the nucleation barriers, which determine hysteretic phase transformations, can be defined.

We explore capillary condensation of fluid in a spherical pore with attractive solid walls. This is the simplest system that exhibits the general features of phase transitions in small volumes. Spherical geometry allows the system to be considered as a whole without imposing periodic boundary conditions. As a typical example, we consider a LJ fluid in a pore of diameter of 15.8σ (σ being the molecular diameter of LJ fluid). The parameters of the fluid−fluid and fluid−solid interactions were chosen to mimic sorption of nitrogen at nitrogen boiling temperature on silica to allow for the opportunity of potential comparison of simulation results with adsorption experiments on mesoporous materials. A spherical pore of 15.8σ can accommodate about 1500 molecules in a liquidlike state. However, as shown in Figures 1 and 2, even such a "large" system cannot be treated as a macroscopic one from the statisticomechanical standpoint since the results of simulations in the canonical ensemble (CE) and the grand canonical ensemble (GCE) are strikingly different.

The paper is structured as follows. The specifics of hysteretic phase transformations in open small systems displayed in grand canonical ensemble Monte Carlo (GCMC) simulations are discussed in section 2. From this discussion we derive three general conclusions: (i) the disappearance of hysteresis above the critical temperature of hysteresis, T_{ch}, has a dynamic rather then a thermodynamic nature and is not related to the vapor−liquid criticality of confined fluid, (ii) spontaneous transitions are determined by the conditions of nucleation, which may differ significantly in laboratory experiments and in GCMC simula-

* Author for correspondence, aneimark@triprinceton.org.

10.1021/jp056407d CCC: $33.50
Published on Web 04/21/2006

tions, and (iii) the critical temperature of hysteresis, T_{ch}, is not a characteristic of the system itself but rather a characteristic of the experimental/simulation conditions of system equilibration. The main objective of this paper is to show how the specifics of phase transformations in open small systems, which are observed in both experiments and simulations, can be interpreted using a statisticomechanical analysis of the close system in the canonical ensemble.

In section 3, we classify the phase behavior in a small system, which exhibits hysteresis in GCMC simulations, using the CE isotherms generated with the gauge cell MC method.[23,44] Using the terminology of the van der Waals theory of phase transitions, we introduce the definitions of phase equilibrium and criticality in a small system. The critical temperature T_{cc} is defined as the temperature that separates monotonic (at $T > T_{cc}$) and nonmonotonic (at $T > T_{cc}$) CE isotherms. We show that the conditions of metastable equilibrium and stable vapor−liquid equilibrium (VLE) are determined by the canonical work function, which is related to the work of formation of one CE state from another. Here, VLE is defined by the Maxwell rule. The hysteretic behavior of practical GCMC isotherms from the positions of constrained equilibrium is examined in section 4. The difference between the GCE and CE isotherms is thoroughly discussed. We introduce the constrained grand thermodynamic potentials of vaporlike and liquidlike states. We show that the true (unconstrained) GCE isotherm can be constructed from the CE isotherm. In section 5, we calculate the energy barriers separating the basins of vaporlike and liquidlike states. We conclude that the hysteretic behavior and the critical temperature T_{ch} of the transition from hysteresis to reversibility are determined by the height of the nucleation barrier, which can be crossed at given experimental/simulation conditions. Within the temperature range, $T_{ch} < T < T_{cc}$, GCMC sampling spans the whole configuration space. Thus, T_{ch} corresponds to the transition from constrained to unconstrained equilibrium. The results are summarized in section 6. The simulation details are given in Appendix 1. In Appendix 2, we present a thorough discussion of the differences in thermodynamic equations based on GCE and CE quantities.

2. Phase Transformations in Grand Canonical Ensemble MC Simulations

Figure 1 presents the results of GCMC simulations at different temperatures. The potential parameters of fluid−fluid intermolecular interactions were chosen to correspond to model nitrogen, and the solid−fluid potential represented interaction of nitrogen with silica. This model system had been studied in our previous works.[42,44] A brief description of the potential parameters and the details of simulation technique are given in Appendix 1. The system in GCMC simulation is open. It is considered to be in equilibrium with an infinite reservoir of bulk vapor thus mimicking experimental conditions of adsorption measurements. At high temperatures, which are larger than a certain temperature T_{ch} called the *hysteresis critical temperature*,[22,35,36] the simulated isotherms are monotonic and reversible. At lower temperatures, $T < T_{ch}$, the isotherms exhibit a prominent hysteresis loop with two stepwise transitions. The ascending adsorption branch corresponds to the vaporlike states obtained in a series of consecutive simulations with a monotonically increasing vapor pressure. As the vapor pressure increases, the fluid is progressively adsorbed at the pore wall, forming a film, which bounds a vapor "bubble" in the pore core. A stepwise transition from a low-density vaporlike state to a high-density liquidlike state

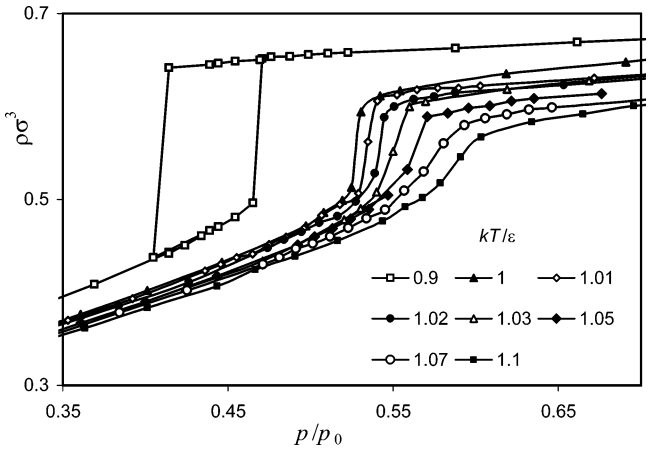

Figure 1. Temperature dependence of capillary condensation isotherms in an open system: transition from hysteresis ($T < T_{ch}$) to reversibility ($T > T_{ch}$). GCMC simulation of a LJ fluid in a spherical pore of diameter $D = 15.8\sigma$ (interaction parameters for LJ model of N_2 in 5.54 nm silica pore). The average fluid density $\rho = 6N/(\pi D^3)$ normalized by σ^3 is presented as a function of the relative pressure in the vapor phase, p/p_0. The isotherms shown (left to right): $kT/\epsilon = 0.9, 1.0, 1.01, 1.02, 1.03, 1.05, 1.07, 1.1$. Hysteresis critical temperature $T_{ch} = 101.5$ K ($kT_{ch}/\epsilon = 1.00$).

reflects spontaneous capillary condensation. Upon condensation, the whole pore is filled by liquidlike fluid, which consolidates as the vapor pressure increases further. The descending desorption branch corresponds to the liquidlike states obtained in a series of consecutive simulations with a monotonically decreasing vapor pressure. Spontaneous evaporation is manifested by a stepwise transition, which occurs at a lower vapor pressure than that of spontaneous condensation. It is associated with the cavitation of a bubble in the stretched metastable liquid.[46]

The GCMC isotherms presented in Figure 1 are qualitatively similar to the experimental isotherms on mesoporous materials of various origin, including samples with spheroidal pores.[25,45] Starting with the works of Everett[18,19] and Ball and Evans,[35] the capillary condensation hysteresis is traditionally considered as a signature of the first-order vapor−liquid transition and its disappearance at elevated temperatures is related to the achievement of the so-called pore critical temperature T_{cc}, which depends on the pore size and shape and is smaller than the bulk critical temperature T_c. Thus, it is implied that $T_{cc} = T_{ch}$. However, experimental works[20−22] and simulation studies of capillary condensation in cylindrical pores[32,36] have shown that the disappearance of hysteresis does not indicate the achievement of criticality and $T_{ch} < T_{cc}$. In the range of temperatures, $T_{ch} < T < T_{cc}$, capillary condensation occurs reversibly.

Indeed, hysteresis manifested in GCMC simulation at $T < T_{ch}$ shows that despite lack of effective constraints during the course of simulation, the sampling was confined either to the basin of low-density states or to the basin of high-density states. Everett[18,32,36] named this irreversible behavior a *permanent* hysteresis, emphasizing that the hysteresis loop is reproducible in repeatable adsorption−desorption cycles and does not depend on the observation time t_{obs} within a wide yet finite practical range. Here, we deal with long-living metastable states separated from the stable states by insurmountable, at given simulation (experimental) conditions, energy barriers. The permanent hysteresis takes place in *practical* simulations and experiments when the simulation (observation) time t_{obs} is, on one hand, much larger than the time t_{loc} of relaxation to a given metastable state (local equilibrium) and, on another hand, much smaller

than the time t_{nucl} of nucleation of the stable phase, which increases exponentially with the height of the nucleation barrier ΔW_n, $t_{loc} \ll t_{obs} \ll t_{nucl} \sim \exp(\Delta W_n/kT)$. That is, the spontaneous condensation and evaporation transitions are determined by the observation time and the conditions of nucleation (i.e., by unavoidable in experiments fluctuations of external parameters such as temperature and pressure), which are essentially different in laboratory experiments and GCMC simulations. If the simulation run was "infinite", and the sampling would include the whole configuration space, the isotherm would be reversible with a condensation step, shifted and rounded as compared with the bulk vapor−liquid equilibrium. An example of such a "*true*" GCE isotherm, which crosses the hysteresis loop formed by *practical* GCMC isotherm, is given below in Figure 4.

3. Phase Equilibrium and Criticality in the Canonical Ensemble

Let us consider the system, which exhibits hysteresis in GCE, as a close system in the canonical ensemble (CE). For a given (N,V,T) state, the *canonical chemical potential* is defined as the incremental difference of the Helmholtz free energies of the systems with $N+1$ and N molecules at fixed V and T

$$\mu_{CE}(N) = F(N+1,V,T) - F(N,V,T) \qquad (1)$$

This definition is consistent with the Widom insertion method,[46] which is widely used in MC simulations to measure the chemical potential in bulk systems. However, practical applications of the Widom method and related techniques for construction of sorption isotherms in nanopores can result in large uncertainties because of the well-known difficulties associated with determination of the chemical potential in small and highly inhomogeneous systems.[47] In this work we employed the gauge cell MC simulation method, which was introduced by us earlier[43] and elaborated in the recent paper.[44] In the gauge cell method, the sample system is connected with a finite reservoir of particles (gauge cell), which serves as a meter of chemical potential. The simulation is performed simultaneously in two cells, which are in chemical equilibrium at isothermal conditions. Mass exchange between the cells is allowed; however, the cell volumes are kept unchanged. The density fluctuations in the pore are controlled by the capacity of the gauge cell. In the limit of infinite capacity, the gauge cell method is equivalent to the GCMC method. In the limit of vanishing capacity, it is equivalent to the canonical ensemble MC (CEMC) method. Choosing the ratio of the gauge cell and pore volumes to be sufficiently small, one can stabilize the fluid in the pore cell in a state, which would be unstable during the contact with the bulk. Thus, the gauge cell has two functions: to prevent the undesirable growth or decay of nuclei and to measure the chemical potential of the pore fluid.

A series of CE isotherms generated with the gauge cell MC method at different temperatures is presented in Figure 2. These isotherms represent the true CE isotherms, which would be obtained in unconstrained CE simulation with independently determined, according to eq 1, chemical potential. It is worth noting that the results of simulations do not depend on the size of the gauge cell. A canonical isotherm, $\mu_{CE}(N)$, represents the chemical potential being a function of the number of particles in the system at fixed volume V and temperature T. Provided the sampling in MC simulation at given N spans the whole configuration space, the canonical isotherm $\mu_{CE}(N)$ is a single valued function. However, as seen from Figure 2, the inverse

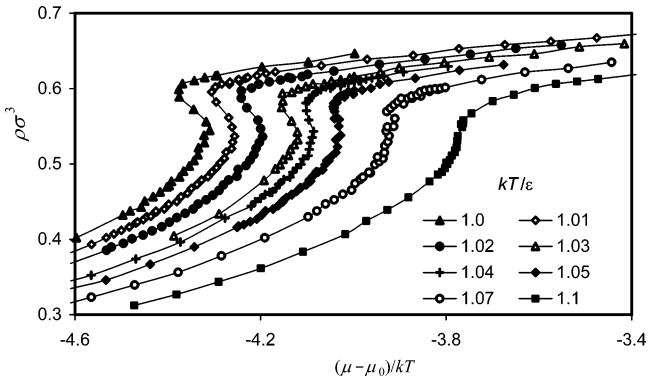

Figure 2. Temperature dependence of capillary condensation isotherms in a closed system: transition from subcritical behavior ($T < T_{cc}$) to supercritical reversibility ($T > T_{cc}$). CE isotherms generated with the gauge cell MC simulation method. The average fluid density $\rho = N/(\pi D^3/6)$ normalized by σ^3 is presented as a function of the relative chemical potential, $(\mu - \mu_0)/kT$. The isotherms shown (left to right): $kT/\epsilon = 1.0, 1.01, 1.02, 1.03, 1.04, 1.05, 1.07, 1.1$. Critical temperature of capillary condensation $T_{cc} = 107.6$ K ($kT_{cc}/\epsilon = 1.062$).

function, $N_{CE}(\mu)$ is single valued only at sufficiently high temperatures. At lower temperatures, the canonical isotherms form sigmoidal loops with a backbending. At a given chemical potential μ, there exist three states, a low-density vaporlike state $N_v(\mu)$, a high-density liquidlike state $N_l(\mu)$, and an intermediate density transient state $N_t(\mu)$, $N_v(\mu) < N_t(\mu) < N_l(\mu)$.

Here, we should make an important comment about the specifics of thermodynamic behavior of small systems compared with their bulk counterparts. Note that sigmoidal isotherms with the backward region of a negative slope, similar to those given in Figure 2, are typical for first-order phase transitions as described by the van der Waals theory and other mean field theories. Moreover, there is a common belief that such van der Waals type isotherms necessarily result from a certain mean field approximation and do not reflect the real equation of state. This is undoubtedly true for the infinite bulk systems in the thermodynamic limit. According to Van Hove's theorem, the averages obtained in the different statistical mechanical ensembles in the thermodynamic limit are the same, and thus, the true equilibrium isotherm in the bulk system must be a single-valued monotonic function with a possible discontinuity at the point of the first-order phase transition. We consider a finite system in which the results of the canonical and the grand canonical ensembles differ, as shown in detail below. While the true equilibrium grand canonical isotherm is a single-valued monotonic function, the true equilibrium canonical isotherm may exhibit a swing that we call a *van der Waals-type loop*. Thus, the van der Waals behavior of the canonical isotherms presented in Figure 2 is not related to a certain mean field approximation; it is a genuine property of small volume systems. All states on the isotherm including the transient states on the backward trajectory with a negative slope are well defined as the states equilibrated in the canonical ensemble. The fact that the small systems in the canonical ensemble behave qualitatively similar to model macroscopic systems with the fluctuations suppressed by a certain mean field approximation was thoroughly discussed in the literature, e.g., by Wales and Doye.[13]

It is worth noticing that van der Waals-type loops were found in the first molecular simulations of phase transitions in small systems.[48] Allen and Tildesley[49] suggested that they be called "small-system" loops to avoid misleading implications of the

van der Waals mean field theory. We obtain the canonical ensemble isotherm by using the gauge cell MC method. As was mentioned above, the results of this method do not depend on the size of the gauge cell and are free of any approximations.[44] The role of the gauge cell is to control the fluctuations in order to stabilize the states which would correspond to the true equilibrium in the close system (canonical ensemble) yet be unstable in the open system (grand canonical ensemble).

Strictly speaking, the canonical isotherm is defined only at integer N. However, given that the number of particles is sufficiently large, one can consider the canonical isotherm as a continuous interpolated function and use integration instead of summation and differentiation instead of finite differences in the respective thermodynamic relations. In the example studied in this paper, the number of particles varies from 0 to 1500, so that the continuous approximation is suitable. This is clearly seen from the examples of discrete CE isotherms given below in Figures 4 and 7. These isotherms were calculated with a precision of one molecule! In view of an inherent scatter of simulation data, interpolation is even desirable. In particular, the chemical potential, which is defined in CE as the difference of the Helmholtz free energies of the systems with $N + 1$ and N molecules at fixed V and T, can be safely calculated as the derivative

$$\mu_{CE}(N) = F(N+1,V,T) - F(N,V,T) \approx \left.\frac{\partial F(N,V,T)}{\partial N}\right|_{V,T} \quad (2)$$

Accordingly, the Helmholtz free energy difference between two states on the canonical isotherm can be calculated by the integration along the isotherm

$$F(N_2,V,T) - F(N_1,V,T) = \sum_{N=N_1}^{N_2-1} \mu_{CE}(N) \approx \int_{N_1}^{N_2} \mu \, dN \quad (3)$$

The terminology of the van der Waals theory of first-order phase transitions and the respective definitions of criticality, binodals, and spinodals are most appropriate for the consideration of phase transformations in small systems using the canonical ensemble isotherms. Here, the *critical temperature* of capillary condensation in the pore, T_{cc}, is unambiguously defined as the temperature, which separates the single-state monotonically increasing "supercritical" isotherms and the multistate sigmoidal "subcritical" isotherms.[32] T_{cc} depends on the pore size and shape and always exceeds the hysteresis critical temperature T_{ch}. With the increase of the pore size, T_{cc} approaches the bulk critical temperature T_c. Thus, in the general case of wetting fluids that is considered here, $T_{ch} < T_{cc} < T_c$. The *spinodals* are defined as the turnover points of subcritical isotherms. The ascending branch of low-density *vaporlike* states is limited by the vaporlike spinodal at the right turnover point of the isotherm, $N_{vs} = N(\mu_{vs})$. The descending branch of high-density *liquidlike* states is limited by the liquidlike spinodal at the left turnover point of the isotherm, $N_{ls} = N(\mu_{ls})$.

The CE treatment allows one to elucidate the definition of *phase equilibrium* in small volume systems at subcritical temperatures, $T < T_{cc}$. Real phase coexistence, or phase separation, as it is defined for macroscopic systems, is impossible inside a small volume system, such as a spherical pore of several nanometers in diameter, due to a prohibitively high energy cost of the interface. Instead, the phase equilibrium can be introduced as the chemical equilibrium between two identical pores containing the states of different density, namely, the vaporlike state N_v in one pore and the liquidlike state N_l in the other, which correspond to the same chemical potential μ

$$\mu_{CE}(N_v) = \mu_{CE}(N_l) \quad (4)$$

Strictly speaking, this equality holds with the precision of one molecule. In small systems, the equilibrium between the two cells is defined in terms of the most probable distribution and is determined by two inequalities, $\mu_{CE}(N_v-1) \le \mu_{CE}(N_l)$ and $\mu_{CE}(N_l-1) \le \mu_{CE}(N_v)$.

To characterize the equilibrium, we introduce an auxiliary function $W_{CE}(N,V,T)$ defined for a given N,V,T state as

$$W_{CE}(N,V,T) = F(N,V,T) - \mu_{CE}(N)N \quad (5)$$

We call $W_{CE}(N,V,T)$ the *canonical work* function, because the difference $\Delta W_{2,1} = W_{CE}(N_2,V,T) - W_{CE}(N_1,V,T)$ determines the work of formation of the state with N_2 particles from the state with N_1 particles. Note $W_{CE}(N,V,T)$ is defined in CE; it should not be confused with the grand thermodynamic potential $\Omega(\mu,V,T)$ defined in GCE. At the supercritical conditions, $W_{CE}(N,V,T)$ approaches $\Omega(\mu_{CE}(N),V,T)$ as the system size increases. In the subcritical region, the functions $W_{CE}(N_v,V,T)$ and $W_{CE}(N_l,V,T)$ defined for vaporlike and liquidlike states approximate the grand thermodynamic potentials $\Omega_v(\mu_{CE}(N_v),V,T)$ and $\Omega_l(\mu_{CE}(N_l),V,T)$ constrained to the basins of vaporlike and liquidlike states, respectively (see Appendix 2).

In general, the condition of equality of chemical potentials (4) determines the *metastable equilibrium* between vaporlike and liquidlike states. Metastable equilibrium implies that the reversible work of formation of one state from the other is not zero, $\Delta W_{vl} = W_{CE}(N_v(\mu),V,T) - W_{CE}(N_l(\mu),V,T) \neq 0$. The reversible work is positive when we transit from the stable state to the metastable state; otherwise, it is negative. The condition of the vanishing reversible work of transition determines the *vapor−liquid* equilibrium (VLE). Thus defined, VLE implies the equality of the canonical work functions

$$W_{CE}(N_v(\mu_{VLE}),V,T) = W_{CE}(N_l(\mu_{VLE}),V,T) \quad (6a)$$

that is equivalent to the *Maxwell rule of equal areas*, which reads in the integral form as

$$\oint_{\mu_{VLE}} N \, d\mu = 0 \quad (6b)$$

The integral form of the Maxwell rule (6b) holds for sufficiently large systems such as the system considered in this paper. For smaller systems, it should be replaced by $\sum_{N=N_v}^{N_e-1}(\mu_{CE}(N) - \mu_{VLE}) = 0$, where μ_{VLE} fulfills the inequalities, $\mu_{CE}(N_v-1) < \mu_{VLE} \le \mu_{CE}(N_l)$ and $\mu_{CE}(N_l-1) < \mu_{VLE} \le \mu_{CE}(N_v)$.

Equation 6 applied to the canonical isotherm determines the equilibrium chemical potential at a given temperature, $\mu_{VLE}(T)$, and the respective vaporlike and liquidlike states, $N_v(\mu_{VLE})$ and $N_l(\mu_{VLE})$. Determined from the set of CE isotherms given in Figure 2, the phase diagram of LJ fluid confined to a 15.8σ spherical pore is given in Figure 3a. To make a comparison with the bulk systems more transparent, we plot the phase diagram as a temperature dependence of the equilibrium fluid densities, $\rho_{v/l} = N_{v/l}/V$. The densities are reckoned from the median density, $\rho_{median} = 1/2(\rho_v + \rho_l)$, that makes the binodal line symmetric. The binodal line is parabolic in the vicinity of the critical point $kT_{cc}/\epsilon = 1.062$. It exhibits a typical classical scaling with exponent $^1/_2$ as seen from Figure 3b, where we

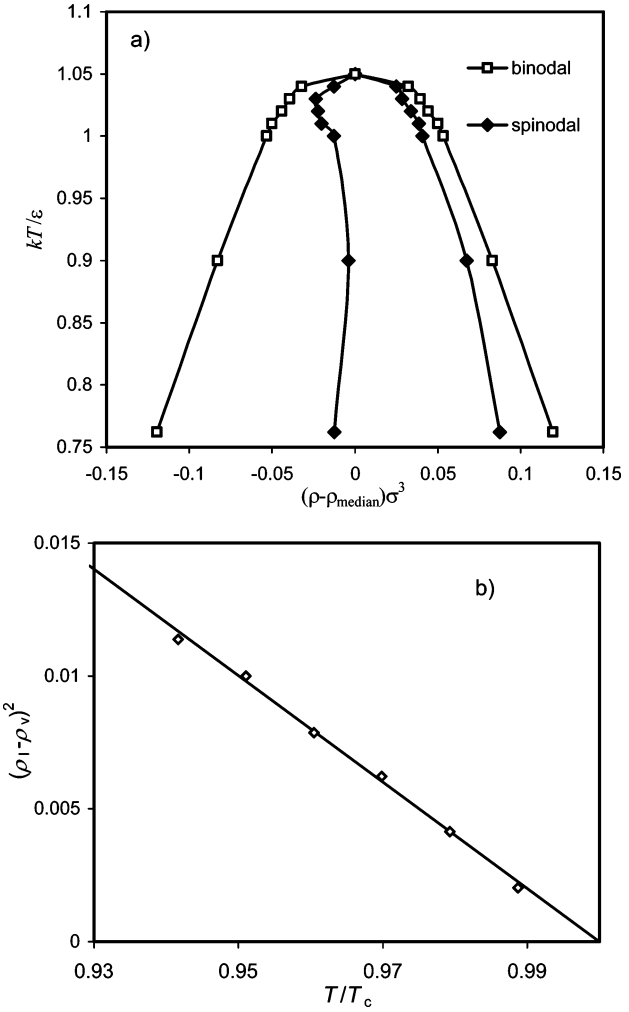

Figure 3. Phase diagram of LJ fluid confined to a 15.8σ spherical pore: (a) binodal and spinodal lines, the critical temperature $kT_{cc}/\epsilon = 1.062$; (b) semilogarithmic plot of the density contrast, $(\rho_l - \rho_v)$, vs the reduced temperature, T/T_{cc}, demonstrating the classical scaling inherent to the phase transitions in finite volume systems.

plot the temperature dependence of the order parameter, $\rho_l - \rho_v$

$$(\rho_l - \rho_v) \propto (1 - T/T_{cc})^{1/2} \tag{7}$$

Note that the classical behavior with the critical exponent $^1/_2$ is a genuine property of any finite volume system revealed in the canonical ensemble, while in macroscopic systems it is attributed to a certain mean field approximation. The spinodal line (Figure 3a) is highly asymmetric since the spinodal densities are reckoned from the median density.

4. Analysis of Hysteretic GCE Isotherms

Examination of CE isotherms helps understand the hysteretic behavior of *practical* GCE isotherms at subcritical temperatures and the transition from hysteresis to reversibility. A detailed comparison of CE and GCE isotherms below the hysteresis critical temperature is presented in Figure 4 for $kT/\epsilon = 0.9$. The practical hysteretic GCE isotherm, $\bar{N}(\mu)$, was generated in the standard GCMC simulation with 1 mln steps per point. The CE isotherm, $\mu_{CE}(N)$, was generated in the ideal gas gauge cell (IGGC) simulation[44] with 1 mln steps per point with the precision of one particle! The multiple data points in the vicinity of the vaporlike spinodal were generated in independent IGGC

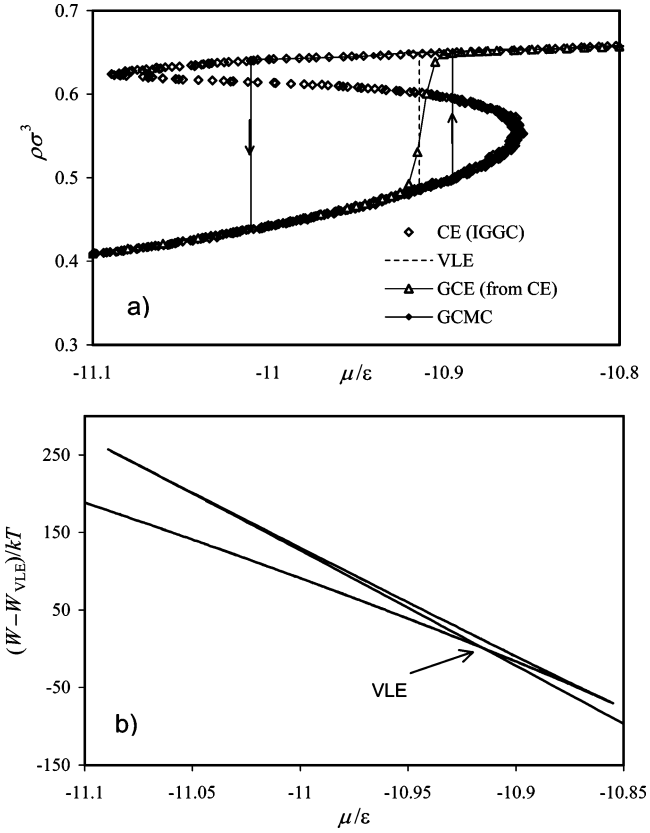

Figure 4. GCE and CE isotherms of LJ fluid confined to a 15.8σ spherical pore at subcritical temperature $kT/\epsilon = 0.9$: (a) Practical hysteretic GCMC isotherm with abrupt condensation and evaporation transitions, CE isotherm generated with the IGGC method, and true GCE isotherm calculated from the CE isotherm (eq 9). The position of VLE is determined from the Maxwell rule (eqs 6). (b) Canonical work function, $W_{CE}(N,V,T)$, plotted against the canonical chemical potential, $\mu_{CE}(N)$. VLE corresponds to the intersection of the vaporlike and liquidlike branches.

simulations. The GCMC and CE isotherm coincide (within the range of inherent simulation errors) for all states generated in GCMC, both stable and metastable, up to the points of spontaneous condensation and evaporation transitions. This means that within the region of hysteresis the GCMC sampling was constrained either to the basin of vaporlike states or to the basin of liquidlike state. These basins are separated by the states of transient density N_t on the backward trajectory of the CE isotherm, which form a watershed on the energy landscape. The energy barriers at the watershed are too high to be crossed during long yet finite simulation runs. In other words, the practical GCMC isotherms of vaporlike, $\bar{N}_v(\mu)$, and liquidlike, $\bar{N}_l(\mu)$, states are obtained at the conditions of constrained equilibrium. $\bar{N}_v(\mu)$ and $\bar{N}_l(\mu)$ represent the averaged numbers of molecules sampled at given chemical potential μ within the basins of vaporlike and liquidlike states, respectively.

The probability to sample (N,V,T) state in GCE at a given chemical potential μ is determined by the function

$$W(N,V,T,\mu) = F(N,V,T) - \mu N \tag{8}$$

which we call below the *deviation potential* in analogy to the similar function employed in ref 52. The deviation potential is a function of four variables: N, V, T, and μ. Minima and maxima of the deviation potential with regard to N at a given chemical potential μ and fixed V and T correspond respectively to the

most and least probable states, which would be sampled in the unconstrained GCE. These states coincide with the states $N_{CE}(\mu)$ on the CE isotherm. Thus, the extrema of the deviation potential equal to the respective canonical work functions $W(N_{CE}(\mu),V,T,\mu) = W_{CE}(N_{CE}(\mu),V,T)$. At subcritical temperatures, the deviation potential $W(N,V,T,\mu)$, as a function of N at given μ, V, and T, has two minima at the vaporlike $N_v(\mu)$ and liquidlike $N_l(\mu)$ states and one minimum at the transient state $N_t(\mu)$. At supercritical temperatures, the deviation potential has one minimum at $N_{CE}(\mu)$.

If the sampling were not constrained and the simulation spanned the whole configuration space, one would obtain the *true* GCE isotherm $N_{GCE}(\mu,V,T)$ as a monotonic function of the chemical potential. The true GCE isotherm can be calculated through the (unconstrained) grand thermodynamic potential

$$\Omega(\mu,V,T) = -kT \ln \sum_N \exp(-W(N,V,T,\mu)/kT) \qquad (9)$$

as

$$N_{GCE}(\mu,V,T) = \frac{\sum_N N \exp(-W(N,V,T,\mu)/kT)}{\exp(-\Omega(\mu,V,T)/kT)} = -\frac{\partial\Omega(\mu,V,T)}{\partial\mu} \qquad (10)$$

Although the true GCE isotherm cannot be sampled in practical GCMC simulations at $T < T_{ch}$, it can be calculated from the CE isotherm via eqs 8−10. The constructed true GCE isotherm is given in Figure 4a. It crosses the hysteresis loop formed by the *practical* GCMC isotherms at the VLE determined by the Maxwell rule (6). The VLE thus defined corresponds to the condition of equal probabilities of sampling the most probable vaporlike and liquidlike states.

The practical hysteretic GCMC isotherms can be expressed through the *constrained grand thermodynamic potentials* for vaporlike, $\Omega_v(\mu,V,T)$, and liquidlike, $\Omega_l(\mu,V,T)$, states, which are defined respectively as

$$\Omega_v(\mu,V,T) = -kT \ln \sum_{N<N_t(\mu)} \exp(-W(N,V,T,\mu)/kT) \qquad (11a)$$

and

$$\Omega_l(\mu,V,T) = -kT \ln \sum_{N<N_t(\mu)} \exp(-W(N,V,T,\mu)/kT) \qquad (11b)$$

Provided that the transient state $N_t(\mu)$ is improbable, the standard statistical mechanical relationships similar to eqs 10 hold for the constrained states

$$\bar{N}_v(\mu) = -\frac{\partial\Omega_v(\mu,V,T)}{\partial\mu} \qquad (12a)$$

and

$$\bar{N}_l(\mu) = -\frac{\partial\Omega_l(\mu,V,T)}{\partial\mu} \qquad (12b)$$

Using the constrained grand thermodynamic potentials, the true GCE isotherm can be expressed as

$$N_{GCE}(\mu,V,T) = \frac{\bar{N}_v(\mu)\exp(-\Omega_v(\mu,V,T)/kT) + \bar{N}_l(\mu)\exp(-\Omega_l(\mu,V,T)/kT)}{\exp(-\Omega_v(\mu,V,T)/kT) + \exp(-\Omega_l(\mu,V,T)/kT)} \qquad (13)$$

Equation 13 shows that the sampling probabilities of low-density and high-density states are determined by the respective constrained grand thermodynamic potentials, $\Omega_v(\mu,V,T)$ and $\Omega_l(\mu,V,T)$. This leads to the *alternative definition of VLE* from the equality of the constrained grand thermodynamic potentials

$$\Omega_v(\mu_{VLE},V,T) = \Omega_l(\mu_{VLE},V,T) \qquad (14)$$

Equation 14 implies the equality of sampling probabilities of any low-density and high-density states in the unconstrained GCE rather then the equality of sampling probabilities of most probable states implied by eq 6. Definition (14) corresponds to the standard definition of phase equilibrium in macroscopic phases. Although it is widely used in the literature for calculating capillary condensation equilibrium in pores,[30] its applicability for small systems cannot be taken for granted. Equations 6 and 14 are identical only in the large volume limit.

For the relatively large system considered here, the mean density insignificantly deviates from the most probable density, $\bar{N}_v(\mu) \approx N_v(\mu)$ and $\bar{N}_l(\mu) \approx N_l(\mu)$. Respectively, the constrained grand thermodynamic potentials (11) insignificantly deviate from the canonical work functions $W_{CE}(N_v(\mu),V,T)$ and $W_{CE}(N_l(\mu),V,T)$. The latter can be reliably estimated by thermodynamic integration along the continuous CE isotherm. However, these deviations cannot be ignored in eqs 13 and 14; see Appendix 2.

5. Nucleation Barriers and Transition from Hysteresis to Reversibility

The canonical work function is instrumental in defining the energy barriers of phase transitions. The plot of the variation of the canonical work function $W_{CE}(N_{CE}(\mu),V,T)$ along the CE isotherm is given in Figure 4b. The intersection of the vaporlike and liquidlike branches determines the position of VLE; for the sake of convenience $W_{CE}(N_{CE}(\mu),V,T)$ is reckoned from its VLE value, W_{VLE}. The upper branch of $W_{CE}(N_{CE}(\mu),V,T)$ corresponds to the transient states on the backward trajectory of the CE isotherm, $N_t(\mu)$. The energy barriers for the transitions between vaporlike and liquidlike states can be estimated through the work of formation of the transient states, which represent critical nuclei of the new phase[46]

$$\Delta W_{vl} = W_{CE}(N_t(\mu),V,T) - W_{CE}(N_v(\mu),V,T) \qquad (15a)$$

$$\mu \geq \mu_{VLE}$$

$$\Delta W_{lv} = W_{CE}(N_t(\mu),V,T) - W_{CE}(N_l(\mu),V,T) \qquad (15b)$$

$$\mu \leq \mu_{VLE}$$

Here subscripts vl and lv denote vapor-to-liquid and liquid-to-vapor transitions, respectively.

The nucleation barriers ΔW_{vl} and ΔW_{vl} calculated with eq 15 for different temperatures are given in Figure 5. At a

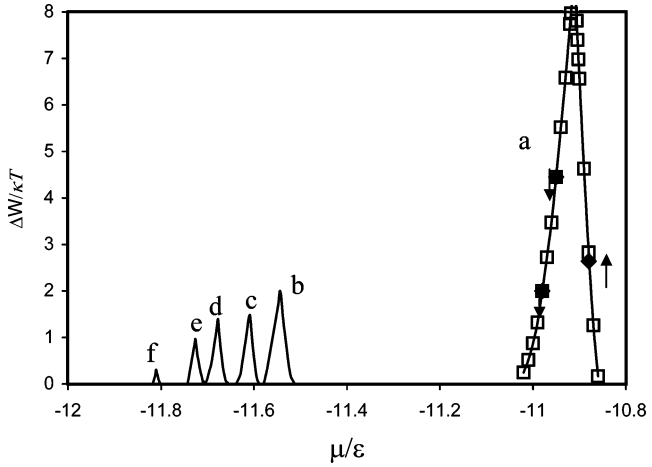

Figure 5. Nucleation barriers at different temperatures: $kT/\epsilon = 0.9$ (a), 1.00 (b), 1.01 (c), 1.02 (d), 1.03 (e), 1.04 (f). Results of calculations with eqs 15. Right and left branches of the cusp correspond to the nucleation barriers of metastable vapor−stable liquid and metastable liquid−stable vapor transitions, respectively. The nucleation barriers vanish at the spinodals and achieve maximum at VLE, where $\Delta W_{vl} = \Delta W_{lv} = \Delta W_{VLE}$ (top of the cusp). The nucleation barrier ΔW_{VLE} vanishes at the critical temperature, $kT_{cc}/\epsilon = 1.062$. The height of the barrier at VLE determines the conditions of hysteresis in practical GCE simulations. Spontaneous vapor−liquid and liquid−vapor transitions observed at $kT/\epsilon = 0.9$ are marked by solid dots and arrows.

subcritical temperature, the nucleation barrier vanishes at the spinodals and achieves a maximum at VLE, where $\Delta W_{vl} = \Delta W_{lv} = \Delta W_{VLE}$. The nucleation barrier ΔW_{VLE} vanishes at the critical temperature T_{cc}. The decrease of the energy barriers approaching the critical temperature is illustrated in Figure 6, where we plot the deviation potential $W(N,V,T,\mu)$ at $\mu = \mu_{VLE}(T)$. Equal minima, W_{VLE}, correspond to the equilibrium vaporlike and liquidlike states, $N_v(\mu_{VLE})$ and $N_l(\mu_{VLE})$; maximum corresponds to the transient state, $N_t(\mu_{VLE})$, and determines the nucleation barrier ΔW_{VLE}. Plots in Figure 6 are reckoned from the VLE value W_{VLE}.

The height of the barrier at VLE determines the conditions of hysteresis in practical GCE simulations. Within the simulation runs of 1 mln steps, it was possible to cross the barriers of several kT whereas the barrier of $10kT$ was not accessible. Thus, the hysteresis critical temperature T_{ch} is determined by the length of the simulation run and the height of the nucleation barrier. For the example considered in this work, the hysteresis critical temperature was estimated as $kT_{ch}/\epsilon \approx 1.00$. Although the maximum energy barrier at $kT/\epsilon = 0.9$ did not exceed $10kT$, the hysteresis was prominent and the vapor−liquid and liquid−vapor transitions occurred irreversibly by crossing the energy barriers of 3 ± 1 kT.

Within the range of temperatures, $T_{ch} < T < T_{cc}$, the GCMC isotherms are reversible because the energy barriers separating the basins of vaporlike and liquidlike states are small enough to be crossed many times back and forth during the simulation run. As a typical example, we present the isotherm at $kT/\epsilon = 1.02$ in Figure 7. As seen from Figure 7b, even in the vicinity of VLE, where the nucleation barriers are maximal, the sampling spans both basins of the configuration space. The probability distribution is bimodal. The maxima correspond to the most probable equilibrium vaporlike and liquidlike states, $N_v(\mu)$ and $N_l(\mu)$, and the minimum corresponds to the least probable transient state, $N_t(\mu)$. The frequency of transitions is shown in Figure 7c. In this case, the GCMC isotherm represents the true GCE isotherm and can be reconstructed from the CE isotherm via eq 10 or eq 13. The result of reconstruction coincides with the reversible isotherm generated in GCMC simulation (Figure 7a) thus confirming that the GCMC sampling included the whole configuration space.

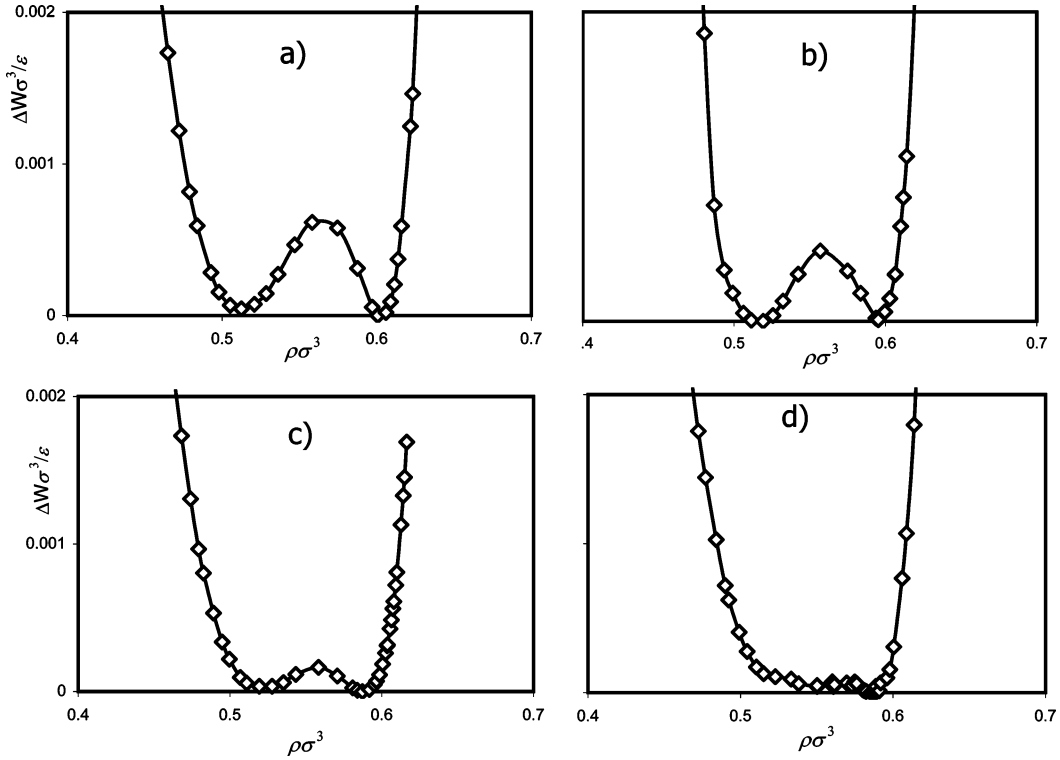

Figure 6. Evolution of the energy barriers approaching the critical temperature. $kT/\epsilon = 1.0$ (a), 1.01 (b), 1.04 (c), 1.05 (d). The deviation potential $W(N,V,T,\mu) = F(N,V,T) - \mu N$ at $\mu = \mu_{VLE}(T)$ is reckoned from its equilibrium value $W_{VLE}(\mu)$. Minima $\Delta W = 0$ correspond to the equilibrium vaporlike and liquidlike states; maximum $\Delta W = \Delta W_{VLE}$ corresponds to the transient state and determines the energy barrier.

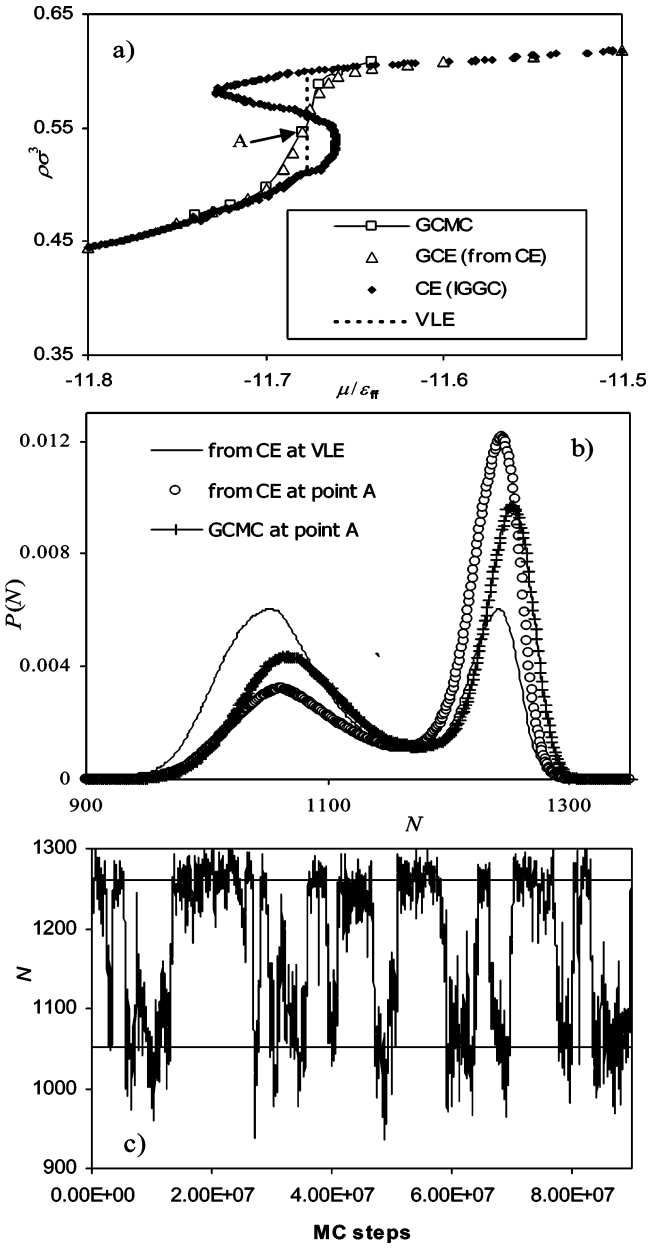

Figure 7. GCE and CE isotherms of LJ fluid confined to a 15.8σ spherical pore at subcritical temperature, $kT/\epsilon = 1.02$. (a) Practical GCMC isotherm is monotonic and reversible, CE isotherm generated with the IGGC method, and true GCE isotherm calculated from the CE isotherm (eq 9). The position of VLE is determined from the Maxwell rule (eqs 6). (b) Probability distributions of the number of particles in GCE: the distribution calculated from the CE isotherm at VLE exhibits equal maxima; the distributions in point A near VLE collected in GCMC simulation run and calculated from the CE isotherm slightly deviate. (c) Fluctuation of the number of molecules during the GCMC run at point A.

At supercritical temperatures, $T > T_{cc}$, the GCE and CE isotherms are almost indistinguishable. However, the density fluctuations in GCMC simulations cannot be ignored in smaller systems containing tens of molecules,[44] where the difference between the GCE and CE isotherms can be appreciable.

6. Conclusions

Drawing on the example of a LJ fluid confined to a spherical pore of 15.8σ with attractive walls, we have shown that the specifics of phase transitions in small systems, which are observed in laboratory experiments and in simulations, can be explained by analyzing the system in the canonical ensemble. The analysis is based on the temperature dependence of CE isotherms. The CE isotherm represents the canonical chemical potential (1) as a function of the number of particles. Here, the critical temperature T_{cc} is defined as the lower limit of temperatures, at which the CE isotherms are monotonic. At subcritical temperatures $T < T_{cc}$, the CE isotherms exhibit sigmoidal van der Waals-type loops. The equilibrium between low-density vaporlike states and high-density liquidlike states is defined by the equality of the canonical work functions that corresponds to the Maxwell rule of equal areas applied to the CE isotherm. In the vicinity of the critical temperature, binodal and spinodal lines constructed from the set of CE isotherms exhibit a classical behavior that is a genuine property of any small volume system. At subcritical temperatures, there is a drastic difference between CE and GCE isotherms. Practical GCMC isotherms are monotonic and reversible only above a certain temperature T_{ch} called the hysteresis critical temperature. At $T < T_{ch}$, practical GCMC isotherms are hysteretic since the sampling is constrained either to the basin of vaporlike states or to the basin of liquidlike states. The conditions of hysteresis and the hysteretic critical temperature are determined by the height of the energy barrier between the basins of vaporlike and liquidlike states. The nucleation barriers can be estimated by the canonical work functions calculated from the CE isotherm. Within the temperature range, $T_{ch} < T < T_{cc}$, the nucleation barriers are small and, within the course of GCMC simulation, the system jumps over the barrier back and forth scanning the whole configuration space. This results in reversible monotonic isotherms.

The keystone of the proposed approach is the construction of CE isotherms. This is hindered by well-known difficulties in the calculation of the chemical potential in small and highly inhomogeneous systems.[47] We constructed CE isotherms with the recently developed gauge cell MC simulation method.[43,44] The gauge cell method allows determination of the continuous subcritical CE isotherm with high precision, necessary for further thermodynamic calculations, which involve its differentiation and integration. The methodology presented in this work can be applied to phase transformations in different systems confined to nanoscale boundaries, including clusters and films, and can be extended to multicomponent supramolecular systems confined to flexible boundaries, such as cells and vesicles.

Acknowledgment. The work was supported by the John Simon Guggenheim Memorial Foundation and the TRI/Princeton exploratory research program. A part of this research was performed at Princeton University, where one of us (A.V.N.) worked in 2004−2005 as a Guggenheim Fellow. A.V.N. thanks George Scherer for his hospitality and fruitful discussions.

Appendix 1. Simulation Details

We consider equilibrium configurations of a LJ fluid in a spherical pore of 5.8σ (σ being the effective molecular diameter) in width with attractive LJ walls. The interaction parameters were chosen to mimic nitrogen at its normal boiling temperature of 77.4 K within a pore typical for silica mesoporous molecular sieves of cagelike structure. The LJ parameters for nitrogen were $\sigma = 0.36154$ nm and $\epsilon/k = 101.5$K.[50] The solid−fluid interactions were represented by the integrated LJ potential induced by the structureless spherical layer of oxygen atoms with solid−fluid parameters $\rho_s\epsilon_{sf}/k = 2253$ K/nm^2, $\sigma_{sf} = 0.317$ nm (ρ_s is the surface density of attractive centers). This model

was employed in a series of our earlier works on modeling capillary condensation in cylindrical and spherical mesopores.[23,32,36] It was shown to provide excellent agreement with experimental data on mesoporous molecular sieves.[23,32] The pore size of 15.8σ, or 5.54 nm, corresponds to the average "internal" pore diameter of a sample of HMM-3 material with *Pm*3*n* cubic symmetry.[51] This system was recently considered in ref 52 where we studied mechanisms of capillary condensation in ink-bottle pores. For a detailed description of fluid−fluid and fluid−solid potentials and simulation protocols, see ref 52.

In all GCMC simulations[53] we followed the standard scheme.[49] No configuration bias was applied. One insertion and one removal were attempted per each trial displacement. The maximum displacement step was adjusted to get the success rate close to $^1/_2$. Wherever only one phase could be observed over a simulation course, the total number of trial MC moves was about 200 000 per molecule and the statistics were collected over the last 100 000 configurations. If a system exhibited oscillations between liquidlike and vaporlike states and the hystogram $P(N)$ had to be obtained, the statistics were collected over 300 000 configurations.

The canonical ensemble isotherms at $kT/\epsilon = 0.9$ and 1.02 were calculated with the precise "ideal gas gauge cell" (IGGC) technique with the precision of one molecule.[44] We performed a series of simulations gradually increasing the total number of molecules from 0 in increments of 20 and keeping size of the gauge so that the average number of molecules in the gauge cell was 20. Where several values of μ were obtained for the same N from overlapping simulation runs, we selected the results from the runs where the total number of configurations with particular N was greater. Overall, one trial molecule insertion into the pore cell from the gauge into and one trial removal from the pore cell were attempted per each attempted displacement. The sequence of attempted insertions and removal was random, which is essential in the gauge cell method.

For all other isotherms we employed a simpler "mean density gauge cell" (MDGC) version,[43] which gives satisfactory results for systems that are large enough and for this pore in particular.[44] The total number of trial MC moves was about 100 000 per molecule. The gauge cell size was adjusted to keep the average number of molecules in the gauge close to 35.

Appendix 2. The Difference between the Grand Thermodynamic Potential, the Constrained Grand Thermodynamic Potential, and the Canonical Work Function

It is necessary to appreciate the difference between the canonical work function $W_{CE}(N,V,T)$ defined in CE and the grand thermodynamic potential $\Omega(\mu,V,T)$ defined in GCE. Let us consider systems with an appreciable number of molecules ($N \gg 100$) and assume that the Helmholtz free energy can be approximated by keeping the quadratic term in the Taylor expansion series. In so doing, the deviation potential can be approximated in the supercritical (one phase) region as

$$W(N_{CE}(\mu)+n,V,T,\mu) \approx W_{CE}(N(\mu),V,T) + \frac{1}{2}k_T^{-1}n^2/N \quad \text{(A1)}$$

In eq 12, we introduced the isothermal compressibility through the standard formula

$$k_T = \left(N\frac{\partial \mu_{CE}}{\partial N}\bigg|_{V,T}\right)^{-1} \quad \text{(A2)}$$

which implies differentiation of the CE isotherm $N_{CE}(\mu)$.

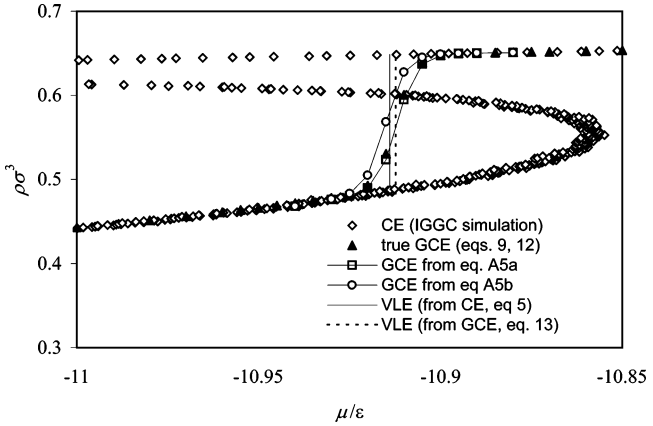

Figure 8. Reconstruction of GCE isotherms from CE isotherms (LJ fluid confined to 15.8*s* spherical pore at subcritical temperature $kT/\epsilon = 0.9$). CE isotherm was generated with the IGGC method. GCE isotherms were calculated from the CE isotherm using an exact eq 10, or equivalently eq 13, and approximations given by eqs A5a and A5b. Note the perfect agreement between the exact data and the results of eq A5, which takes into account the differences of compressibilities of vaporlike and liquidlike states. Deviation between the positions of VLE defined from CE isotherms (eq 5) and GCE isotherms (eq 13) is $\Delta\mu_{VLE} = 0.005kT$.

Consequently, the grand thermodynamic potential is given by

$$\Omega(\mu,V,T) \approx W_{CE}(N_{CE}(\mu),V,T) - kT\ln\sqrt{2\pi NkTk_T} \quad \text{(A3)}$$

In the subcritical (two-phase) region, eq A1 is applied to the constrained grand thermodynamic potentials, which can be related to the respective canonical work functions through the isothermal compressibilities of vaporlike and liquidlike states, $k_T(N_v)$ and $k_T(N_l)$, defined by eq A2

$$\Omega_v(\mu,V,T) \approx W_{CE}(N_v(\mu),V,T) - kT\ln\sqrt{2\pi kTN_vk_T(N_v)} \quad \text{(A4a)}$$

$$\Omega_l(\mu,V,T) \approx W_{CE}(N_l(\mu),V,T) - kT\ln\sqrt{2\pi kTN_lk_T(N_l)} \quad \text{(A4b)}$$

Employing eqs A4, the true GCE isotherm (13) can be calculated through the quantities readily available from an interpolated CE isotherm,

$$N_{GCE}(\mu) \approx \{N_v(\mu)\exp[-W_{CE}(N_v(\mu),V,T)/kT] + N_l(\mu)\exp[-W_{CE}(N_l(\mu),V,T)/kT]\sqrt{N_lk_T(N_l)/N_vk_T(N_v)}\}\Big/ \{\exp[-W_{CE}(N_v(\mu),V,T)/kT] + \exp[-W_{CE}(N_l(\mu),V,T)/kT]\sqrt{N_lk_T(N_l)/N_vk_T(N_v)}\} \quad \text{(A5a)}$$

Note that accounting in eq A5a for the difference in compressibilities of vaporlike and liquidlike states is essential. The intuitively suitable approximation, which neglects the dispersion of GCE sampling around the most probable state and assumes that

$$\Omega_{v/l}(\mu,V,T) \approx W_{CE}(N_{v/l}(\mu),V,T)$$

$$N_{GCE}(\mu) \approx \{N_v(\mu)\exp[-W_{CE}(N_v(\mu),V,T)/kT] + N_l(\mu)\exp[-W_{CE}(N_l(\mu),V,T)/kT]\}\Big/ \{\exp[-W_{CE}(N_v(\mu),V,T)/kT] + \exp[-W_{CE}(N_l(\mu),V,T)/kT]\} \quad \text{(A5b)}$$

gives an appreciable discrepancy with eq A5a. This is shown in Figure 8 with the example of subcritical isotherms at $kT/\epsilon =$

0.9. At the same time, the results of the exact eq 13, which is equivalent to eq 10, and the approximate eq A5a are in perfect agreement.

Within the approximation (A4), the difference between the positions of VLE defined by eqs 6 and 14 can be evaluated as

$$\Delta\mu_{\mathrm{VLE}} = \frac{kT}{(N_{\mathrm{l}} - N_{\mathrm{v}})} \ln \frac{N_{\mathrm{v}} k_T(N_{\mathrm{l}})}{N_{\mathrm{l}} k_T(N_{\mathrm{l}})} \qquad \text{(A6)}$$

Since the slope of the vaporlike branch is larger than that of the liquidlike branch, $\Delta\mu_{\mathrm{VLE}}$ is positive: VLE defined through eq 13 is located at a somewhat larger chemical potential than that defined through eq 5. For the system considered here, $\Delta\mu_{\mathrm{VLE}} = 0.005kT$ at $kT/\epsilon = 0.9$; see Figure 8. As the system size increases, $\Delta\mu_{\mathrm{VLE}}$ diminishes as $1/N$.

It is worth noting that for many systems with more then a hundred particles there is no practical difference between the use of constrained grand thermodynamic potentials and canonical work functions in calculations of VLE and true GCE isotherms. However, the above discussion is essential for a better understanding of the importance of the rigorous methodology for interpretation of hysteretic phase transitions.

References and Notes

(1) Lebowitz, J. L.; Percus, J. K. *Phys. Rev.* **1961**, *124*, 1673.
(2) Hill, T. L. *J. Chem. Phys.* **1962**, *36* (12), 3182.
(3) Hill, T. L. *Thermodynamics of Small Systems, Parts I and II*; W.A. Benjamin, Inc.: New York, 1963.
(4) Penrose, O.; Lebowitz, J. L. In *Fluctuation Phenomena*; Montroll, E., Lebowitz, J. L., Eds.; North-Holland: Amsterdam, 1987; Chapter 5.
(5) Hill, T. L. *Nano Lett.* **2001**, *1* (3), 111.
(6) Wales, D. J.; Berry, R. S. *Phys. Rev. Lett.* **1994**, *73* (21), 2875.
(7) Borrmann, P.; Mulken, O.; Harting, J. *Phys. Rev. Lett.* **2000**, *84* (16), 3511.
(8) Mulken, O.; Stamerjohanns, H.; Borrmann, P. *Phys. Rev. E* **2001**, *64* (4), 047105.
(9) Gross, D. H. E. *Microcanonical thermodynamics. Phase transitions in "Small" Systems*; World Scientific: Singapore, 2001.
(10) Gulminelli, F.; Chomaz, P. *Phys. Rev. E* **2002**, *66* (4), 046108.
(11) Chomaz, P.; Gulminelli, F. *Nucl. Phys. A* **2005**, *749*, 3C.
(12) Wales, D. J.; Berry, R. S. *J. Chem. Phys.* **1990**, *92* (7), 4473.
(13) Wales, D. J.; Doye, J. P. K. *J. Chem. Phys.* **1995**, *103* (8), 3061.
(14) Gross, D. H. E.; Madjet, M. E. *Z. Phys. B*: *Condens. Matter* **1997**, *104* (3), 541.
(15) Chbihi, A.; Schapiro, O.; Salou, S.; Gross, D. H. E. *Eur. Phys. J. A* **1999**, *5* (3), 251.
(16) Gelb, L. D.; Gubbins, K. E.; Radhakrishnan, R.; Sliwinska-Bartkowiak, M. *Rep. Prog. Phys.* **1999**, *62* (12), 1573.
(17) Schmidt, M.; Kusche, R.; Hippler, T.; Donges, J.; Kronmuller, W.; von Issendorff, B.; Haberland, H. *Phys. Rev. Lett.* **2001**, *86* (7), 1191.
(18) Everett, D. H. In *The Solid−Gas Interface*; Flood, E. A., Ed.; Marcel Dekker: New York, 1967; Vol. 2.
(19) Burgess, C. G. V.; Everett, D. H.; Nuttall, S. *Pure Appl. Chem.* **1989**, *61* (11), 1845.
(20) Branton, P. J.; Hall, P. G.; Sing, K. S. W.; Reichert, H.; Schuth, F.; Unger, K. K. *J. Chem. Soc., Faraday Trans.* **1994**, *90* (19), 2965.
(21) Ravikovitch, P. I.; Odomhnaill, S. C.; Neimark, A. V.; Schuth, F.; Unger, K. K. *Langmuir* **1995**, *11* (12), 4765.
(22) Morishige, K.; Shikimi, M. *J. Chem. Phys.* **1998**, *108* (18), 7821.
(23) Neimark, A. V.; Ravikovitch, P. I.; Vishnyakov, A. *Phys. Rev. E* **2000**, *62* (2), R1493.
(24) Morishige, K.; Ito, M. *J. Chem. Phys.* **2002**, *117* (17), 8036.
(25) Morishige, K.; Tateishi, N. *J. Chem. Phys.* **2003**, *119* (4), 2301.
(26) Morishige, K.; Tateishi, N.; Fukuma, S. *J. Phys. Chem. B* **2003**, *107* (22), 5177.
(27) Maeda, N.; Israelachvili, J. N.; Kohonen, M. M. *Proc. Natl. Acad. Sci. U.S.A.* **2003**, *100* (3), 803.
(28) Morishige, K.; Iwasaki, H. *Langmuir* **2003**, *19* (7), 2808.
(29) Maddox, M. W.; Gubbins, K. E. *J. Chem. Phys.* **1997**, *107* (22), 9659.
(30) Peterson, B. K.; Gubbins, K. E. *Mol. Phys.* **1987**, *62* (1), 215.
(31) Miyahara, M.; Kanda, H.; Shibao, M.; Higashitani, K. *J. Chem. Phys.* **2000**, *112* (22), 9909.
(32) Vishnyakov, A.; Neimark, A. V. *J. Phys. Chem. B* **2001**, *105* (29), 7009.
(33) Radhakrishnan, R.; Gubbins, K. E.; Sliwinska-Bartkowiak, M. *J. Chem. Phys.* **2002**, *116* (3), 1147.
(34) Evans, R.; Marconi, U. M. B.; Tarazona, P. *J. Chem. Soc., Faraday Trans. Ii* **1986**, *82*, 1763.
(35) Ball, P. C.; Evans, R. *Langmuir* **1989**, *5* (3), 714.
(36) Neimark, A. V.; Ravikovitch, P. I.; Vishnyakov, A. *J. Phys.*: *Condens. Matter* **2003**, *15* (3), 347.
(37) Doye, J. P. K.; Wales, D. J. *J. Chem. Phys.* **1995**, *102* (24), 9673.
(38) Gulminelli, F.; Chomaz, P. *Phys. Rev. Lett.* **1999**, *82* (7), 1402.
(39) Gross, D. H. E.; Votyakov, E. V. *Eur. Phys. J. B* **2000**, *15* (1), 115.
(40) Chomaz, P.; Gulminelli, F. *Phys. A (Amsterdam, Neth.)* **2003**, *330* (3−4), 451.
(41) Gonzalez, A.; White, J. A.; Roman, F. L. *J. Chem. Phys.* **1998**, *109* (9), 3637.
(42) Neimark, A. V.; Vishnyakov, A. *J. Chem. Phys.* **2005**, *122* (5), 054707.
(43) Neimark, A. V.; Vishnyakov, A. *Phys. Rev. E* **2000**, *62* (4), 4611.
(44) Neimark, A. V.; Vishnyakov, A. *J. Chem. Phys.* **2005**, *122* (23), 234108.
(45) Ravikovitch, P. I.; Neimark, A. V. *Langmuir* **2002**, *18* (25), 9830.
(46) Widom, B. *J. Chem. Phys.* **1963**, *39* (11), 2808.
(47) Frenkel, D.; Smit, B. *Understanding Molecular Simulation. From Algorithms to Applications*; Academic Press: San Diego, CA, 1996.
(48) Alder, B. J.; Wainwright, T. E. *Phys. Rev.* **1962**, *127* (2), 359.
(49) Allen, M. P.; Tildesley, D. J. *Computer simulation of liquids*; Clarendon Press: Oxford, 1987.
(50) Ravikovitch, P. I.; Vishnyakov, A.; Russo, R.; Neimark, A. V. *Langmuir* **2000**, *16* (5), 2311.
(51) Guan, S.; Inagaki, S.; Ohsuna, T.; Terasaki, O. *J. Am. Chem. Soc.* **2000**, *122* (23), 5660.
(52) Vishnyakov, A.; Neimark, A. V. *Langmuir* **2003**, *19*, 3240.
(53) Norman, G. E.; Filinov, V. S. *High Temp.* **1969**, *7* (2), 216.